EXPERIMENTAL STUDY OF ROTOR GROUND EFFECT IN LOW-DENSITY ENVIRONMENT

Vellingiri Ramanujam R
Indian Institute of Technology Madras
Chennai, India

Rohith M
Indian Institute of Technology Madras
Chennai, India

Ajo Jospeh Anto
Indian Institute of Technology Madras
Chennai, India

Ranjith Mohan
Indian Institute of Technology Madras
Chennai, India

ABSTRACT

Ground effect is a widely studied phenomenon in rotorcraft at standard atmospheric conditions of earth. With increasing interest in flights on Mars and other atmospheric conditions, the ground effect in those environments is a pertinent question. The current work is focused on experimental study of a rotor in low atmospheric densities in ground effect. Measured thrust and torque are reported, and the results at different densities are compared. A significant effect of recirculation is observed in the rotor performance due to the confined space of the low-density chamber.

INTRODUCTION

The ground effect phenomenon refers to the enhancement in thrust (under constant power conditions) experienced by a rotor when operating close to the ground surface. Rotor ground effect has been investigated for several decades, both numerically and experimentally. Several works were reported for various rotor configurations in hover, such as propellers/ proprotors (Refs. 1 and 2), single-rotor helicopters, coaxial rotors (Refs. 3, 4), tandem (Refs. 5–7) and quad-rotor (Refs. 8 and 9). The effect of rotor parameters such as twist and tip geometry were also investigated in the works of Refs. 10 and 11. While all the previous works provided valuable insights into the aerodynamics of the rotors at standard atmospheric conditions, there remains a gap in understanding its behavior in low-density environments which include applications in high-altitude regions and extraterrestrial atmospheres such as Mars. With recent interest in using helicopter/rotorcraft for Mars exploration and success of 'Ingenuity Mars helicopter' experimental works (Refs. 12–16) has been done on rotors operating in low-density conditions. These hover experiments were performed in a closed vacuum/environmental chamber, where the closed chamber walls surrounding the rotor in all directions can affect aerodynamics and performance of the rotor. Further, very few works have been reported (Refs. 17–19) on the effect of recirculation on a rotor inside a confined space. This paper presents an experimental study aimed at understanding the effects of rotor ground proximity in low-density environments. The objective is to provide a comprehensive analysis of how decreasing air density affects the in-ground effect (IGE) and out-of-ground effect (OGE) rotor performance parameters, such as thrust and power. In a specialized vacuum chamber that replicates low-density conditions, a series of controlled experiments were conducted to measure rotorcraft performance parameters and compared these data with theoretical models and results from standard atmospheric conditions.In addition, the effect of recirculating flow inside the confined low-density chamber is also reported.

METHODOLOGY

The details of the experimental setup used for this study is explained below.

Experimental Setup

Figure 1 shows the vacuum chamber used for the investigation of ground effect in a low-density environment. The chamber is a 2.4m cubic structure made of steel. The working fluid inside the chamber is atmospheric air (primarily N_2). In this work, low densities are simulated in the chamber up to a value of $0.0175\ \mathrm{kg/m^3}$ which corresponds to the average surface atmospheric density on Mars (Ref. 20). An $120\ \mathrm{m^3/hr}$ oil-sealed vacuum pump is used to reduce the pressure level inside the vacuum chamber. Air density is calculated using the measurement of pressure, temperature, and humidity of air inside the chamber. Air temperature inside the chamber is found to be almost the same as the ambient temperature outside the chamber due to thermal conduction of vacuum chamber walls. Humidity level reduces with decrease in pressure and is found

Presented at 50th European Rotorcraft Forum, Marseille, France, 10-12 September, 2024

Figure 1: $2.4m \times 2.4m \times 2.4m$ Vacuum chamber

to be around 10% at 16 mBar.

The rotor test rig used in this study consists of 1) adjustable height stand 2) test rotor/propeller+BLDC motor 3) motor drive and electronics and 4) six-axis load cell. The base of the variable height stand is fixed to the bottom level of the vacuum chamber using a rigid frame made of steel. The top/mounting plate of the stand can be raised or lowered using an electric linear actuator with a range of 0.3 m. The position of the mounting plate is achieved by controlling the actuator using a Lab view interface through USB communication with an accuracy of 0.1 mm. Figure 4 shows the picture of the rotor test setup mounted on the variable height stand.

The rotor used for this investigation is a 40 inch (0.508 m radius) off-the-shelf propeller (Fig. 2) with twist and chord variation along the radius. The propeller is also found to have an acceptable Figure of merit (FM) at low Reynolds number conditions, corresponding to Mars atmosphere. The rotor is directly attached to a BLDC motor without any swash plate mechanism. Hence, the rotor/propeller is operated in an untrimmed condition, i.e the rotor torque/thrust is not maintained at a constant value with variation in rotor-ground separation. The rotor speed is maintained at a desired value using an electronic speed controller (ESC), from a PC interface. Other electronics used in the experiment include a temperature sensor and capacitance based humidity sensor for the calculation of air density. Pressure is measured using two different gauges : 1) pressure range, 1 atm to 50 mBar is measured using a Panasonic DP100 pressure transmitter, 2) pressure less than 25 mBar is measured using Edwards CG16K gauge which has higher accuracy for lower pressure measurements. The thrust produced by the rotor and reaction torque are measured at constant rotor angular speed using an ATI Gamma 6-axis load cell. The thrust and torque measurements are acquired and logged into a PC. The logged data are then averaged and reported in the following section for different height and air density combinations.

The ground surface used in this study is a square platform made using a high-density polyurethane (PU) foam board. A dimension of $1.8\text{m} \times 1.8\text{m}$ is used so that the ground surface is almost twice the diameter of the rotor in all directions. The rotor was tested in two different flow configurations: 1) normal and 2) inverted flow configurations. A schematic of the direction of thrust and flow (induced inflow) is shown in Fig. 3. In the normal flow configuration, the rotor produces thrust in the upward direction and induced velocity (hence rotor wake) is in the downward direction. The base of the rotor stand is fixed to the base of the vacuum chamber and not moved for the entire duration of the experiment in this configuration. The foam ground was placed below the rotor using supports as shown in Fig. 4. However, for a given vertical position of the ground, only 300mm ($\Delta h/R = 0.59$) maximum rotor-ground separation could be achieved due to the limitation of the actuator travel. Hence, to achieve ground separation distance ranging from OGE conditions ($h > 2R$) to IGE ($h < 0.2R$) the ground position has to be raised to different levels relative to the base of the test stand. Since a larger ground surface is used, the rise in level of the ground may change the effective volume of the vacuum chamber, which in turn may have variation in recirculating effects on the rotor performance. Hence, to investigate the effect of raising the ground level (change in chamber volume), inverted flow rotor tests were carried out. In this configuration, the rotor thrust is directed downwards, while the wake is directed in the upward direction. The ground surface was fixed permanently at the maximum possible level inside the vacuum chamber using a rigid frame and supports. Only rotor height was changed in this configuration using the variable height stand. The base of the variable height was raised to different levels using a rigid platform of smaller dimensions to cover the $0.2 < h/R < 2$ range (Fig. 5).

Figure 2: T-Motor G40 x 13.1 Propeller

First, ground effect experiments were conducted in the normal flow configuration (i.e. thrust directed upwards) at 1 atm without recirculation effects. The experiment was carried out in the same building where the vacuum chamber is installed, but the rotor test rig was kept sufficiently far away from ceiling and walls of the building so that the rotor wake does not return to the rotor. This experiment was primarily done for the investigation of the recirculation effect inside the vacuum chamber and to find a recirculation factor to make correction in the readings taken inside the closed vacuum chamber. Results are presented in the form of thrust augmentation factor ($\mathrm{K_G}$ factor) and torque ratio. The thrust augmentation factor, $\mathrm{K_G}$ is given by,

$$\mathrm{K_G} = \frac{T}{T^{\infty}} = \frac{C_T}{C_T^{\infty}} \tag{1}$$

where C_T is the rotor thrust coefficient and superscript ∞ denotes the value when the rotor is far from the ground (typically 1 rotor diameter distance). It has to be noted that the $\mathrm{K_G}$

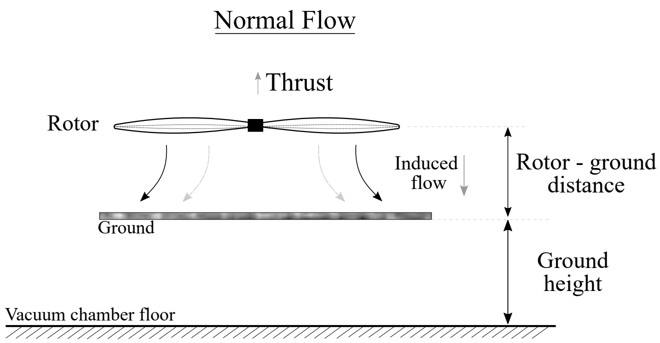

(a) Normal flow rotor configuration

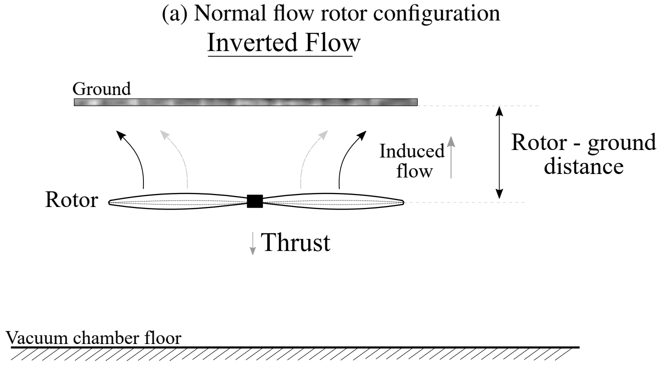

(b) Inverted flow rotor configuration

Figure 3: Schematic of rotor flow

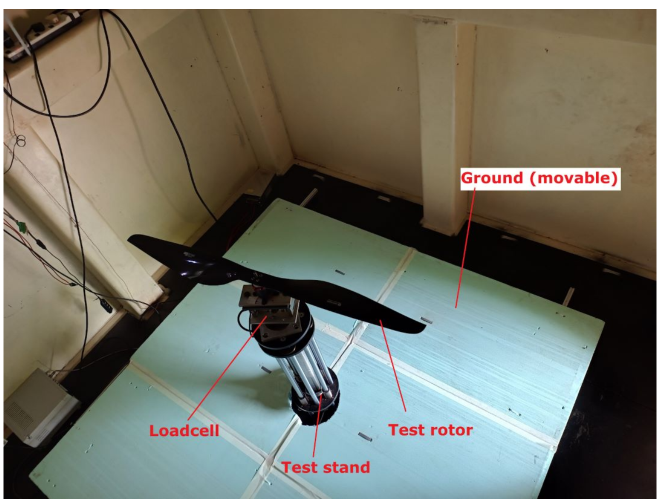

Figure 4: Ground effect setup: Normal flow configuration

factor is defined for a constant rotor power. However, in this work, the rotor power is not maintained at a constant value and its variation with ground distance is reported in a non-dimensional form as follows,

$$\text{power ratio} = \frac{C_P}{C_P^\infty} = \frac{C_Q}{C_Q^\infty} \tag{2}$$

where C_Q is the torque coefficient of the rotor. The experimental values are also compared with standard models of thrust augmentation factors (Refs 22 and 21) and the effect of density (hence Reynolds number) is brought out. The ground effect studies are carried out on the rotor at 4 different pressure (air density) levels of the vacuum chamber, as shown in Table

Figure 5: Ground effect setup: Inverted flow configuration

1. The Reynolds number of the rotor is calculated based on the chord value at the 75% of radius as follows,

$$Re = \frac{\rho V_{0.75} C_{0.75}}{\mu} \tag{3}$$

where $V_{0.75}$ refers to the tangential velocity of the rotor at $0.75R$ and $C_{0.75}$ is the chord of the rotor at $0.75R$. The chord value of the rotor $0.75R$ is found to be 65 mm. The rotor was tested in the Reynolds number range, 10^3–10^5 and Mach number of 0.1 – 0.45. The pressure level inside the chamber was maintained within 0.5 mBar during the experiment for each pressure level in Table 1.

Pressure mBar	air density kgm^{-3}	rotor RPM	Reynolds number at $0.75R$	Tip Mach number
1014	1.10	1000	1.5×10^5	0.15
600	0.67	750 1000	7.2×10^4 9.67×10^5	0.11 0.15
272	0.30	1000 1500	4.1×10^4 6.2×10^4	0.15 0.23
16	0.0175	2000 3000	4.7×10^3 7.0×10^3	0.30 0.45

Table 1: Test parameters

RESULTS AND DISCUSSION

The thrust and torque measurements obtained using the ground effect experimental setup are presented in this section.

Normal flow configuration results

The experimental data obtained for the rotor in normal flow configuration is presented first. Figure 6 shows the variation of thrust and torque of the rotor with rotor-ground distance at 1 atm without any recirculation effects (i.e. outside the vacuum chamber). As mentioned earlier, the results are compared with the standard K_G factors. In the results presented in this paper, 'K_G factor 1' corresponds to the thrust augmentation factor suggested by Ref. 21, which is given by,

$$K_G^1 = 1 + \frac{0.0199}{\frac{h}{R}^2} + \frac{0.0944}{(0.6572 + \frac{h}{R}^2)} \quad (4)$$

and 'K_G factor 2' corresponds to the K_G factor ('Cheeseman factor') suggested by Ref. 22, which is given by the following expression,

$$K_G^2 = \frac{1}{1 - \frac{1}{(4h/R)^2}} \quad (5)$$

The thrust and torque variation in this case is as expected, with monotonous increase in thrust with a decrease in ground height. Similarly, torque values are almost constant until $h/R = 0.5$ and drop with a further decrease in rotor-ground distance. The results presented in Fig. 6 correspond to a rotor speed of 1000 RPM. The K_G factor suggested by Ref. 21 is close to the experimental data in this case. It has to be noted that the K_G factor is usually computed for a constant power or constant thrust of the rotor (i.e trimmed rotor). However, the results presented in this paper correspond to untrimmed rotor as mentioned earlier and the K_G factor results are presented assuming a very small variation in power. Figure 7 shows the performance of the rotor at 1 atm, where the rotor is mounted inside the vacuum chamber. It can be observed that the results do not follow the usual monotonic increase in the thrust with a decrease in the rotor-ground distance (h/R) due to the recirculation of the rotor wake inside the closed chamber. The thrust values decrease until $h/R \approx 0.75$ instead of increasing in the usual manner. The torque values does not have smooth variation with ground separation distance in $0.5 < h/R < 2.5$ region. This region is dominated by recirculation effects, and rotor disk might operate in a climb like scenario rather than in a ground effect. However, a detailed investigation such as CFD studies and wake measurements are required to confirm the above observed trend in measurements. A recirculation factor for thrust and torque (Eqs. 6 and 7) is obtained from the experimental data at 1 atm and presented in Fig. 8.

$$R_{fact}^T = \frac{C_T^{out}(h/R)}{C_T^{in}(h/R)} \quad (6)$$

$$R_{fact}^Q = \frac{C_Q^{out}(h/R)}{C_Q^{in}(h/R)} \quad (7)$$

The above recirculation factors (Eqs. 6 and 7) are used to make corrections in the data obtained inside the vacuum chamber to account for the recirculation effects. It is assumed that the recirculation effects are the same for all air density values, and the same correction factor is used for the low-density results.

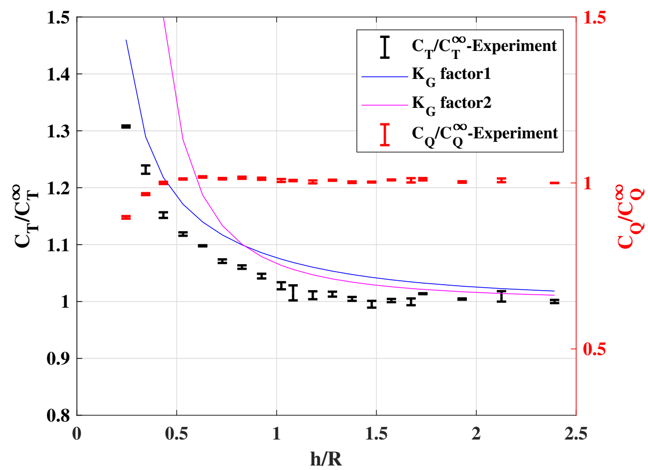

Figure 6: Thrust and torque coefficient of normal flow rotor at 1atm, 1000 RPM (outside vacuum chamber)

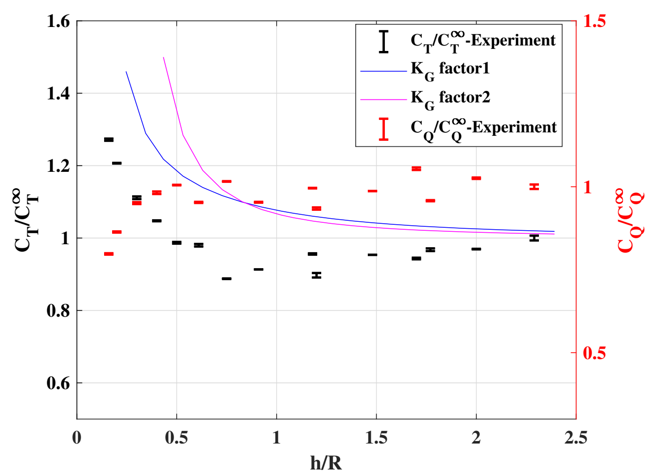

Figure 7: Thrust and torque coefficient of normal flow rotor at 1 atm, 1000 RPM (inside vacuum chamber)

Figures 9–11 show the performance of the rotor in normal flow configuration at densities lower than the ambient atmosphere. In this case also, the thrust variation shows a dip as observed in 1 atm results (Fig. 7) until $h/R \approx 0.75$. Further, a relatively large scatter is also observed in the low-density data compared to the 1 atm case. The increment in thrust with decrease in ground distance (thrust augmentation) is higher in the case of 16 mBar pressure level, as shown in Fig. 11. Also, the rotor power does not drop rapidly when the rotor

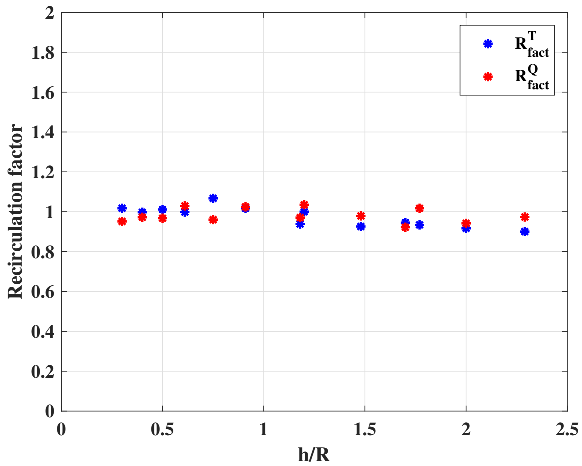

Figure 8: Recirculation factor for the normal flow rotor configuration (1 atm)

comes very close to the ground, as observed in the torque variation with ground distance. The above trend is likely due to the dominance of viscous power at low-density (low-Reynolds number).

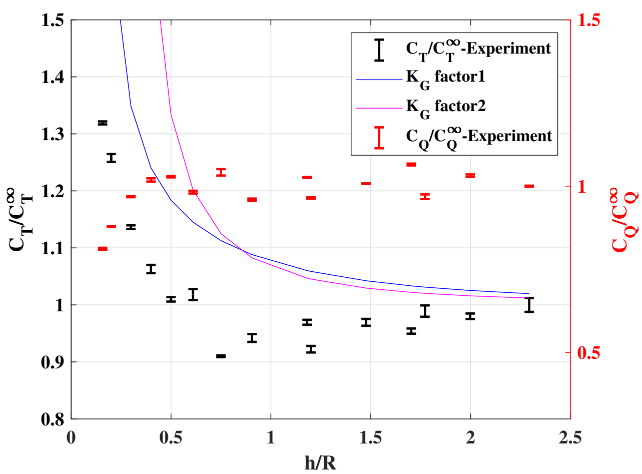

Figure 9: Thrust and torque coefficient of normal flow rotor at 0.6 Bar, 1000 RPM

The correction factor obtained using Fig.8 is applied to the experimental data inside the vacuum chamber at different pressure levels. Figures 12 and 13 show the corrected experimental data at 1 atm and 16 mBar respectively. The corrected data is agreeing well with the K_G factor predicted using Ref. 21.

Inverted flow rotor results

The results obtained using the inverted flow rotor configuration are presented in this section. Figure 14 shows the performance of the rotor at 1 atm inside the vacuum chamber for this rotor configuration. It is assumed that inverted and normal

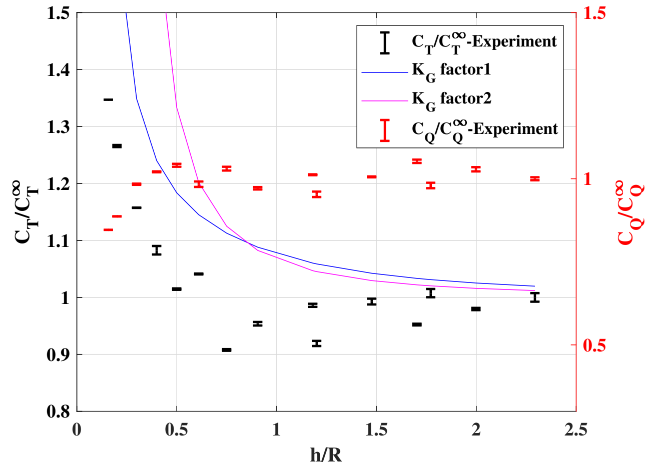

Figure 10: Thrust and torque coefficient of normal flow rotor at 0.3 Bar, 1500 RPM

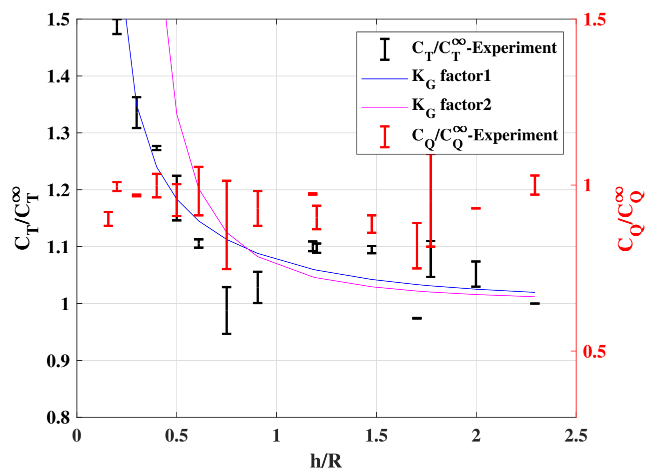

Figure 11: Thrust and torque coefficient of normal flow rotor at 0.016 Bar (2000 RPM)

flow performance of the rotor are the same outside the chamber, without recirculation effects. Hence, a separate experiment was not conducted and results are not presented. A recirculation factor variation with ground distance is presented in Fig. 15 for this rotor configuration. The recirculation factors for the normal rotor and inverted flow rotor configuration show a different trend as observed in Figs 8 and 15.

Figures 16–21 show the performance of the rotor in ground effect at different lower value of air densities. The results of 0.6 and 0.3 Bar pressure levels (Figs. 16–19) are similar to 1 atm results in this rotor configuration also. However, the rate of increase of thrust augmentation factor (K_G factor) with rotor-ground distance appears to be higher for the 0.016 Bar case (Figs. 23 and 21). This is consistent with the results of normal flow rotor configuration presented in the previous section. The power variation presented in Figs. 14, 16–21 show a clear increase in power (hence torque) in the $0.5 < h/R < 2.5$ region of the inverted flow configuration, whereas such a con-

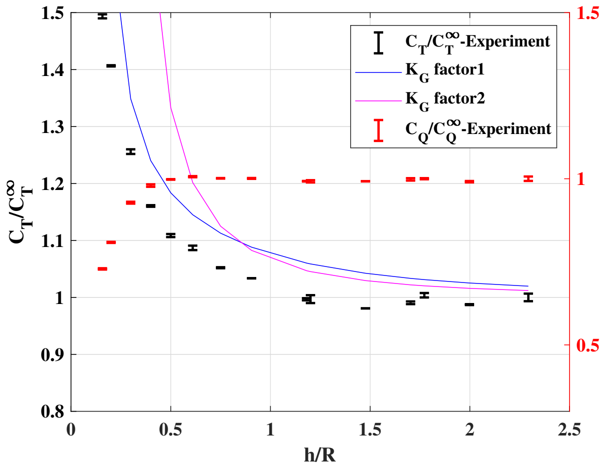

Figure 12: Corrected data of normal flow rotor at 1 atm (1000 RPM)

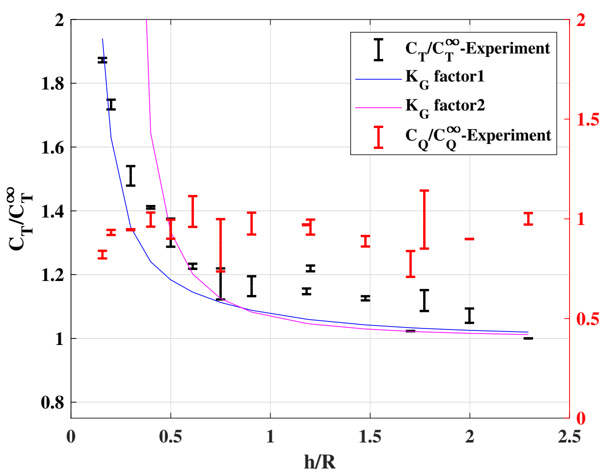

Figure 13: Corrected data of normal flow rotor at 0.016 Bar (2000 RPM)

clusion could not be made in the normal flow configuration results due to large scatter in the data. The rotor power drops when the rotor is very close to the ground ($h/R < 0.5$) for pressure level 1 atm, 0.6 Bar and 0.3 Bar cases as observed in the normal flow configuration. However, the rotor power shows a small increase in power for 16 mBar case, which is likely due to strong viscous effects experienced by the rotor blades as observed in the case of normal flow configuration (Fig. 11).

A corrected data is presented in Figs. 12 and 13 for the 1 atm and 0.016 mBar case respectively using the recirculation factor obtained from Fig. 15. The effect of Reynolds number on the K_G factor is presented in Fig. 24 four different rotor-ground distance where the ground effect dominates ($0.25 < h/R < 1$). It can be observed that the K_G factor increases for lower Reynolds number.

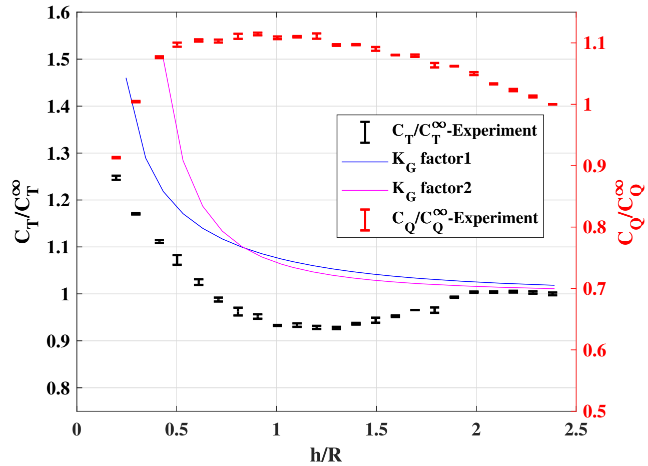

Figure 14: Thrust and Torque coefficient of inverted flow rotor at 1 atm, 1000 RPM

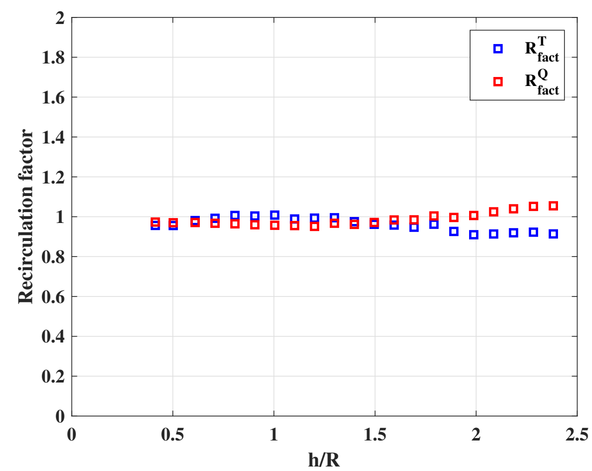

Figure 15: Recirculation factor for the inverted flow rotor at 1 atm

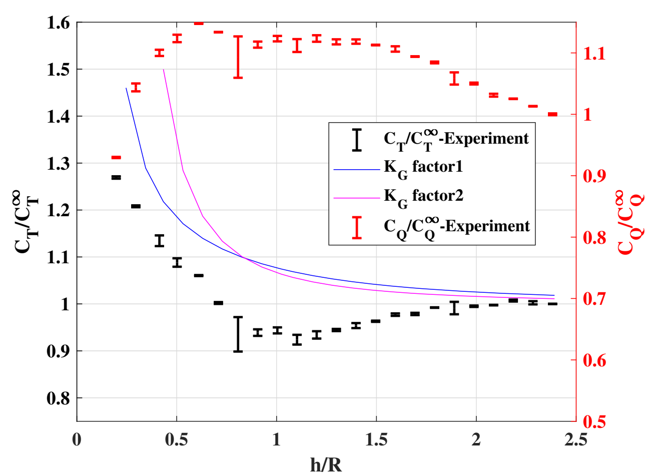

Figure 16: Thrust and Torque coefficient of inverted flow rotor at 0.6 Bar, 750 RPM

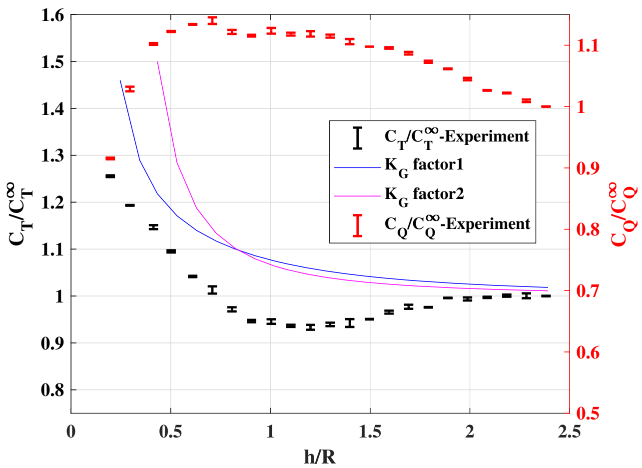

Figure 17: Thrust and Torque coefficient of inverted flow rotor at 0.6 Bar, 1000 RPM

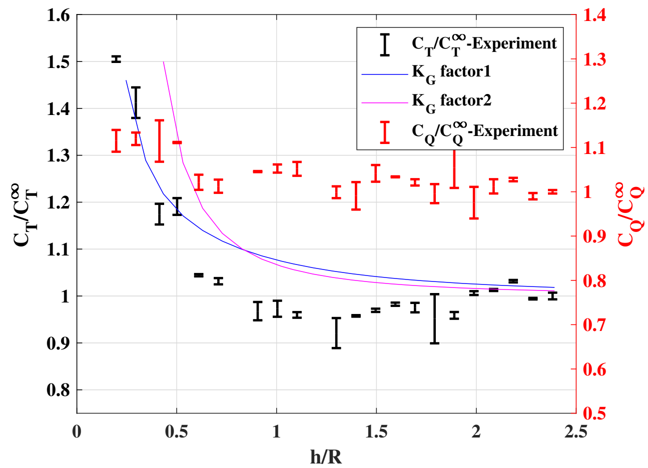

Figure 20: Thrust and Torque coefficient of inverted flow rotor at 0.016 Bar, 2000 RPM

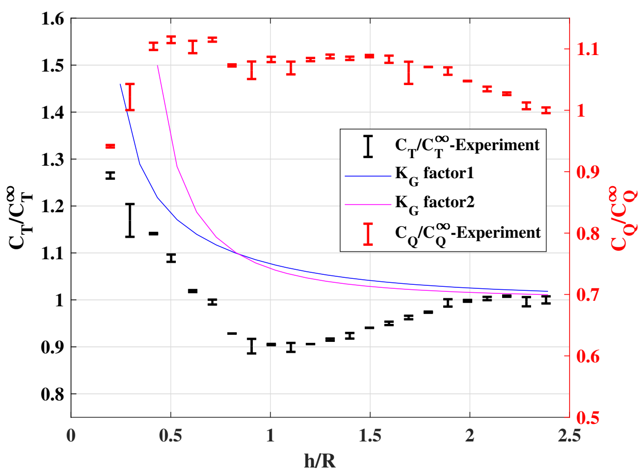

Figure 18: Thrust and Torque coefficient of inverted flow rotor at 0.3 Bar, 1000 RPM

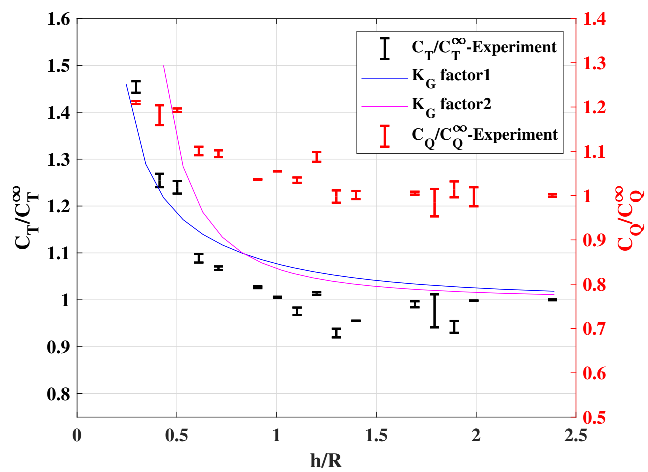

Figure 21: Thrust and Torque coefficient of inverted flow rotor at 0.016 Bar, 3000 RPM

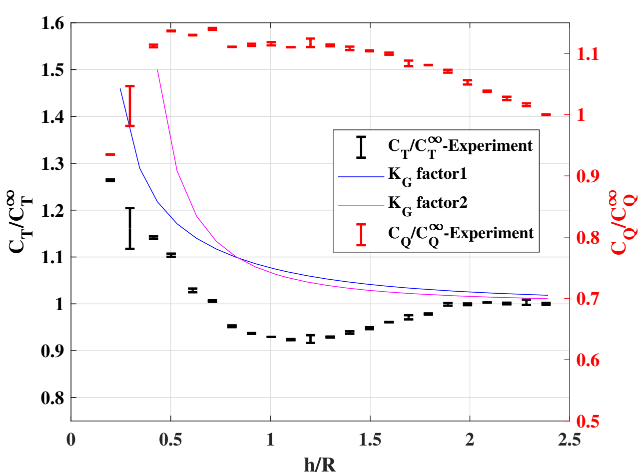

Figure 19: Thrust and Torque coefficient of inverted flow rotor at 0.3 Bar, 1500 RPM

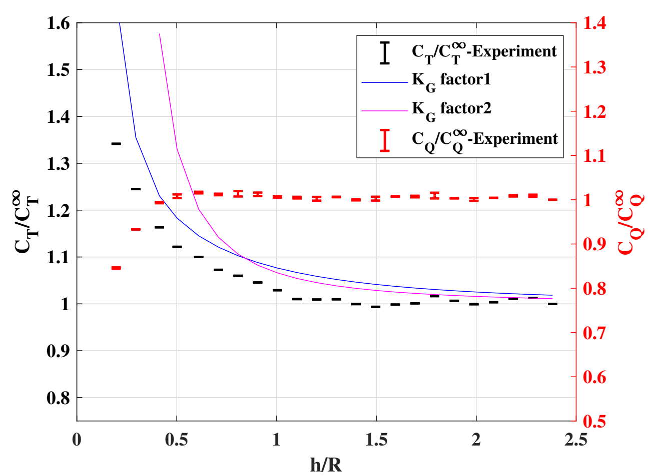

Figure 22: Corrected data of inverted flow rotor at 1 atm, 1000 RPM

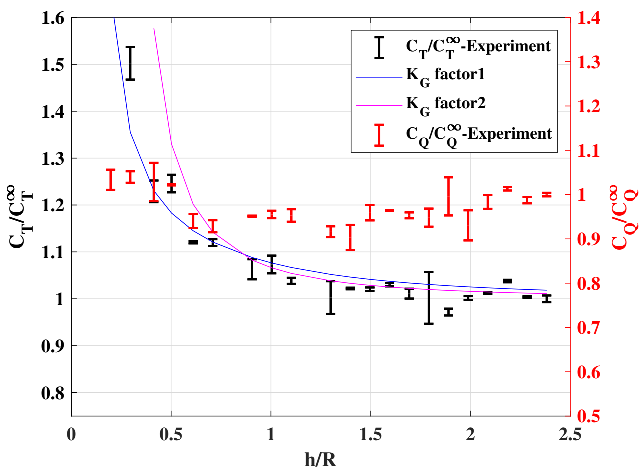

Figure 23: Corrected data of inverted flow rotor at 0.016 Bar, 2000 RPM

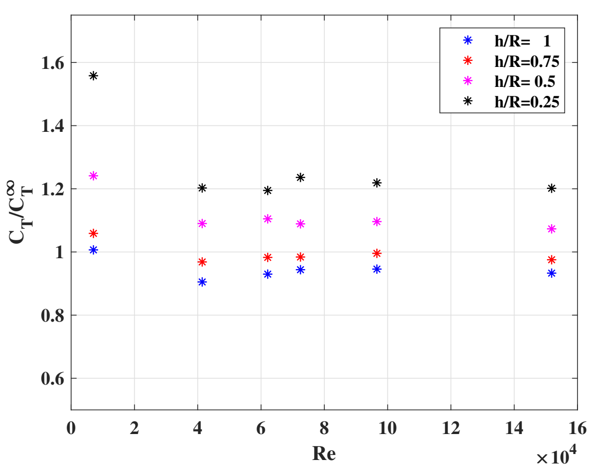

Figure 24: Effect of Reynolds number on thrust augmentation factor of inverted flow rotor

CONCLUSIONS

A series of experiments were conducted to investigate the effect of ground surface below the rotor on aerodynamic performance. The following conclusions are made for the ground effect and recirculation effect on rotors in a confined space :

1. A significant recirculation effect is observed in the hover performance of the rotor inside a closed vacuum chamber, and their effects cannot be neglected for correlation studies.
2. Correction factors were proposed to account for the recirculation effects on the experimental data obtained inside the vacuum chamber. A good agreement with the K_G factor models were obtained after correction.
3. The ground effect in the low-density, low-Reynolds number environment is dominated by viscous effects, as observed in the torque results.
4. The thrust augmentation factor, K_G increases in the low-Reynolds number environment.

Author contact:
Vellingiri Ramanujam R, ramanujam3548@gmail.com
Rohith M, rohithm92@gmail.com
Ajo Joseph Anto, antoajo@gmail.com
Ranjith M, ranjith.m@iitm.ac.in

ACKNOWLEDGMENTS

We thank SERB (Project No. CRG/2022/000959) and DST (Project No. DST/TDT/DDP- 1 4/2O21) for supporting the study. We express our gratitude towards Prof. S. Arul and Mr. Justin (Dept. of Civil Engg., IIT-Madras) for designing the low density chamber. We also thank Mr. Rishi Gogoria for helping to set up the experiments.

REFERENCES

1. Knight, M. and Hefner, R. A., "Analysis of Ground Effect on the Lifting Airscrew," NACA Technical Notes 835, 1941.
2. Betz, A., "The Ground Effect on Lifting Propellers," NACA Technical Memorandum 836, 1937.
3. Lim, J.W., McAlister, K.W., and Johnson, W., "Hover Performance Correlation for Full-Scale and Model-Scale Coaxial Rotors ," *Journal of the American Helicopter Society*, Vol. 54, (3), pp. 32005-32005. '
4. Silwal, L., Bhagwat, M. and Raghav, V., "Aerodynamic Interactions of Counter-Rotating Coaxial Rotors Hovering in Ground Effect," *Journal of Aircraft*, Vol. 59, (6), 2022, pp. 1416-1425.
5. Healy, R., McCauley, J., Gandhi, F., and Sahni, O., "A Computational Examination of Side-by-Side Rotors in Ground Effect," *Journal of the American Helicopter Society*, Vol. 68, (3), 2023, pp. 32007-32024.
6. Ramasamy, M., and Yamauchi, G.K., "Using Model-Scale Tandem-Rotor Measurements in Ground Effect to Understand Full-Scale CH-47D Outwash," *Journal of the American Helicopter Society*, Vol. 62, (1), 2017, pp. 1-14.
7. Dekker, H.N., Ragni, D., Baars, W.J., Scarano, F., and Tuinstra, M., "Aerodynamic Interactions of Side-by-Side Rotors in Ground Proximity" *AIAA Journal*, Vol. 60, (7), 2022, pp. 4267-4277.
8. Otsuka, H., Kohno, M., and Nagatani, K., "Fountain Flow Visualization in Quadrotor Wake Decreasing Rotor Thrust In-Ground Effect" *Journal of Aircraft*, Vol. 61, (3), 2024, pp. 761-773.
9. Tanabe, Y., Sugawara, H., Sunada, S., Yonezawa, K., and Tokutake, H., "Quadrotor drone Hovering in Ground effect" *Journal of robotics and mechatronics*, Vol. 33, (2), 2021, pp. 339-347.

10. Schmaus, J., Berry, B., Gross, W. and Koliais, P., "Experimental Study of Rotor Performance in Deep Ground Effect with Application to a Human-Powered Helicopter," Proceedings of the 68th Annual Forum of the American Helicopter Society, Fort Worth, Texas, 2012.

11. Kalra, T., Lakshminarayan, V.K., and Baeder, J.,"Effect of Tip Geometry on a Hovering Rotor in Ground Effect: A Computational Study," Proceedings of 31st AIAA applied aerodynamics conference, San Diego, CA, pp. 2542, June 2013.

12. Tsuzuki, N., Sato, S. and Abe, T.,"Conceptual Design and Feasibility for a Miniature Mars Exploration Rotorcraft," Proceedings of International Congress of the Aeronautical Sciences, Yokohama, Japan, 29 August-3 September 2004.

13. Shrestha, R., Benedict, M., Hrishikeshavan, V., and Chopra, I.," Hover Performance of a Small-Scale Helicopter Rotor for flying on Mars," *Journal of Aircraft*, Vol. 53, (4), 2016, pp. 1160-1167.

14. Zhao, P., Quan, Q., Chen, S., Yang, T., Bai, D., Tang, D., and Deng, Z., "Geometry shape selection of NACA airfoils for Mars rotorcraft ," *Acta Astronautica*, Vol. 157, 2019: 300-309.

15. Escobar, D., Chopra, I. and Datta, A., "High-Fidelity Aeromechanical Analysis of Coaxial Mars Helicopter," *Journal of Aircraft*, Vol. 58, (3), 2021, pp. 609-623.

16. Ruiz, M.C., Scanavino, M., D'Ambrosio, D., Guglieri, G., and Vilardi, A.," Experimental and numerical analysis of hovering multicopter performance in low-Reynolds number conditions," *Aerospace Science and Technology*, Vol. 128, 2022, pp. 107777.

17. Jardin, T., Prothin, S., and Magaña, C.G., "Aerodynamic Performance of a Hovering Microrotor in Confined Environment," *Journal of the American Helicopter Society*, Vol. 62, (2), 2017, pp. 1-7.

18. Sutkowy Jr, M.L., "Relationship between Rotor Wake Structures and Performance Characteristics over a Range of Low-Reynolds Number Conditions," Master's thesis, The Ohio State University, 2018.

19. McCoy, M., Wadcock, A.J., and Young, L.A., "Documentation of the recirculation in a closed-chamber rotor hover test," NASA/TM-2016-219162, 2016.

20. Koning, W.J., Johnson, W. and Grip, H.F., "Improved Mars Helicopter Aerodynamic Rotor Model for Comprehensive Analyses," *AIAA Journal*, Vol. 57, (9), pp. 3969–3979

21. Joseph, C., and Mohan, R., "A New Ground effect Factor based on Image Vortices", Proceedings of 6th Asian/Australian Rotorcraft Forum and Heli Japan, Kanazawa, Japan, November 2017.

22. Cheeseman, I. and Bennett, W., "The Effect of the Ground on a Helicopter Rotor in Forward Flight," Aeronautical Research Council Reports and Memoranda 3021, 1955.

CLASSIFICATION & COPYRIGHT